Materials Advances

ROYAL SOCIETY OF CHEMISTRY

PAPER

View Article Online
View Journal | View Issue

Cite this: *Mater. Adv.*, 2025, 6, 3648

A lipid hydrogel to transport and release an anti-HIV-1 peptide into vaginal mucosa†

Noèlia Loza-Rodríguez, *[ab] Aina Millán-Sánchez, [a] Aleix Benítez, [c] Ramon Pons, [a] María José Gómara, [d] Isabel Haro, [d] Meritxell Genescà [c] and Olga López*[a]

Received 16th January 2025,
Accepted 21st April 2025

DOI: 10.1039/d5ma00042d

rsc.li/materials-advances

The cervicovaginal mucosa is a main portal of entry for the human immunodeficiency virus (HIV). Peptide antiretroviral therapy is a promising treatment to decrease the HIV infection rate, but yet it presents several weaknesses such as poor bioavailability, development of drug resistance and poor ability to reach the mucosal tissue with the effective concentration. In this work, an HIV inhibitor peptide (RE-E1P47) was encapsulated into a lipidic hydrogel (HG) to test its capacity to deliver the peptide to mucosa *ex vivo* and its pre-exposure prophylactic efficacy to inhibit or limit HIV infection. The proposed HG is made only with lipids and water and has a composition similar to the vaginal fluid that naturally covers the mucosa. Characterization studies with confocal microscopy, ATR-FTIR, SAXS and WAXS reveal that peptide incorporation does not alter the hydrogel's micro- and nanostructure. Permeation and diffusion tests confirm peptide delivery to the surface layers of the mucosal tissue without interaction or diffusion into a vaginal fluid simulant (VFS). Importantly, efficacy studies demonstrate a significant reduction in HIV infection rates of 60% after HG treatment. Thus, we highlight this material formulation as a strong candidate for mucosal topical application, particularly in the development of pre-exposure prophylaxis (PrEP) treatments against HIV-1.

1. Introduction

In the skin, mucosal barriers separate the external environment from the body's internal milieu. These selectively permeable barriers avoid the passage of microorganisms while permitting flux of water, ions and solutes, including nutrients. In the case of the cervicovaginal mucosa, both the cervicovaginal mucus and the stratified squamous epithelium (a nonkeratinized tissue)[1,2] represent major physical barriers that can limit penetration of bacterial infections and potentially life-threatening agents, including human immunodeficiency virus (HIV), the toxin associated with toxic shock syndrome and herpes simplex virus.[1,3] The vagina has been extensively explored as an alternative route of drug administration due to its important advantages such as large contact surface area, good permeability, and high vascularization, to avoid the hepatic first-pass metabolism and provide a high concentration of the drug at the site of action with the reduction of side effects.[4,5] The development of new therapeutic compounds promises significant advances in treating local genital infections; however, many of these compounds may also irritate the tissue leading to inflammation and damage that can compromise the mucosal tissue barrier.[1,6] Thus, paradoxically, a potentially effective therapeutic agent can result in increased vulnerability to infection and disease.

The development of drug delivery systems for the treatment of the vaginal mucosa must consider and respect the environment and the characteristics of the mucosa, as well as attributes that favor its application, such as stability, spreadability and retention in the tissue. Aqueous semisolid gels are currently the most common dosage forms used for vaginal mucosa treatments. They have the potential for vaginal application, by favoring the permanence of the formulation on the vaginal mucosa, which allows reduction of dosages with greater therapeutic efficacy, especially in relation to conventional dosage forms. Among several thickeners, biocompatible polymers with mucoadhesive and thermo-responsive properties have attracted great attention for vaginal drug delivery.[1,3,7] This interaction

[a] *Department of Chemical and Surfactant Technology, Institute of Advanced Chemistry of Catalonia (IQAC-CSIC), C/Jordi Girona 18-26, 08034 Barcelona, Spain. E-mail: noelia.loza@iqac.csic.es, oloesl@cid.csic.es*
[b] *Bicosome S.L., C/Jordi-Girona 18-26, 08034 Barcelona, Spain*
[c] *Infectious Diseases Department, Vall d'Hebron Institut de Recerca (VHIR), Vall d'Hebron Hospital Universitari, Vall d'Hebron Barcelona Hospital Campus, Passeig Vall d'Hebron 119-129, Barcelona, 08035, Spain*
[d] *Unit of Synthesis and Biomedical Applications of Peptides, Institute of Advanced Chemistry of Catalonia (IQAC-CSIC), C/Jordi-Girona 18-26, 08034 Barcelona, Spain*

† Electronic supplementary information (ESI) available. See DOI: https://doi.org/10.1039/d5ma00042d

between the hydrogel and mucosa can be established *via* electrostatic interactions, hydrogen bonds, van der Waals forces and hydrophobic interactions. However, they do not always achieve the retention of the drugs in the mucosa. Thus, the development of new materials that overcome these limitations is a subject of study in the field of biomedicine.[1,7]

A large variety of mucosa drug delivery systems are already in use or under investigation for the treatment of several infections such as bacterial vaginosis, candidiasis, trichomoniasis, HIV, *etc.* These include gels, creams, foams, tablets, capsules, suppositories, pellets, microparticles, nanoparticles, patches, films, or rings.[1,3,7–11] However, these pharmaceutical forms are limited by the vaginal route due to leakage, drug stability, short residence time, and poor release and distribution of drugs in the cervicovaginal cavity. Regarding HIV infection, over the last decade, pre-exposure prophylaxis (PrEP) has proven to be a successful method of preventing HIV-1 sexual transmission. Tenofovir is an effective medicine that is used to treat chronic hepatitis B as well as to prevent and treat HIV/AIDS.[12] Several clinical trials have shown that tenofovir is successful in HIV-1 topical PrEP. The most promising findings were from the CAPRISA 004 clinical study, which showed that a 1% tenofovir vaginal gel decreased HIV infection by roughly 39%.[12] Even though preclinical trials showed promising antiviral results, these systems are rather unreliable since they must be used regularly. Alternatively to small antiretroviral drugs, synthetic peptides have been designed as fusion inhibitors for their use in pre- and post-exposure prophylaxis (PrEP and PEP) of HIV-1 infection.[13] Particularly, a synthetic peptide (E1P47) has been defined as an anti-HIV inhibitor with a broad spectrum of activity against viruses from different clades, subtypes and tropisms and whose interaction with its viral target takes place at the membrane level.[14,15] Polymeric nanoparticles coated with glycol chitosan, lipid raft-like liposomes and peptide amphiphilic-based supramolecular structures have also been developed for the targeted delivery of antiviral peptides to animal and human mucosal tissue explants.[10,16–19] In addition to the use of these nanostructures for targeting the cervicovaginal and anorectal tissues, new topical delivery systems are also being explored.

In previous works, we have developed a colloidal hydrogel (HG) formed exclusively by biological molecules, lipids and water. The characterization of HG was carried out through confocal microscopy studies, ATR-FTIR, SAXS, WAXS and rheology.[20–23] Microscopy studies showed a sponge-like morphology with a supramolecular aggregation of lipid multilamellar vesicles ranging from 5 to 30 μm in diameter coexisting with lipid lamellae. Furthermore, this HG has been demonstrated to promote the retention of hydrophilic and lipophilic molecules in the cutaneous tissue.[20,21,24] In the present work, we report the incorporation of a retro-enantio analog of the E1P47 peptide (RE-E1P47) in this lipidic HG to be delivered into vaginal mucosa.[25] The RE-E1P47 peptide has been structurally designed to maintain the active conformation required for interaction with its viral target site, is highly resistant to human sera proteases and has shown great inhibitory potency in pre-clinical pre-exposure prophylaxis results (PrEP) using human mucosal tissue explant models.[25] However, its retention in the mucosa is very limited. Recent studies regarding the dependance of vaginal mucosa permeability with temperature suggested that the main barrier to drug diffusion was lipoidal in nature and mainly linked to the presence of inter and intracellular granules containing lipid lamellae.[26] The HG is composed by 95% water and 5% of lipids, mimicking the composition of the cervicovaginal mucus (which is 92–95% of water and 5–8% of solid matter, including glycoproteins, proteoglycans, and lipids).[27] Thus, our hypothesis is that the lipidic composition of this HG will enhance peptide retention in the mucosa tissue. Even in the absence of polymers or other gelling molecules, the lipidic HG exhibits adequate rheological and biocompatible properties to facilitate the application of the gel.

In this work, we characterize the microstructure of the lipid HG with the incorporation of the peptide with ATR-FTIR, SAXS, WAXS and fluorescence confocal microscopy. In addition, diffusion experiments were conducted using a vaginal fluid simulant (VFS) to evaluate whether the HG might dilute, interact and diffuse with the vaginal fluid, or undergo structural disruption. The results indicated that while the HG experienced some hydration, there was no diffusion of its components into the VFS. Then, permeation study of the RE-E1P47 labelled with Rhodamine was performed on *ex vivo* ovine vaginal mucosa. Our results indicate that the peptide permeated and was retained in the mucosa in a higher concentration when it was applied with the HG than when it was applied in aqueous solution. Furthermore, it has been observed that the peptide applied with the HG can enter inside the epithelial cells of the mucosa. Finally, a pre-exposure prophylactic efficacy in human cervicovaginal mucosa demonstrated that the HG delivered the required amount of peptide to the mucosa to significantly inhibit *ex vivo* HIV infection after the treatment. Consequently, the HG delivery system presented here represents a promising candidate for delivery of cervicovaginal interventions such as a targeted peptide for PrEP against HIV-1.

2. Materials and methods

2.1. Materials

Hydrogenated soy phosphatidylcholine (HSPC; Phospholipon® 90H) and 1,2-dioleoyl-3-trimethylammonium-propane (DOTAP) were purchased from Lipoid GmbH (Ludwigshafen, Germany). Chloroform was supplied from Carlo Erba Reagents S.A.S. (Val de Reuil, Paris, France), and purified water was obtained by an ultrapure water system, Milli-Q plus 185 (Millipore, Bedford, MA). Phosphate buffered saline tablets (PBS) were supplied by Sigma Aldrich (Merck KGaA, Darmstadt, Germany). Hoechst solution, wheat germ agglutinin (WGA) Alexa Fluor 488 and methylene blue stains were supplied by Thermo Fisher Scientific Inc. Nile red (NR) was purchased from MedChemExpress (USA). FluorSaveTM Reagent was obtained from EMD Millipore Corp., USA. Ovine vaginal mucosa was kindly donated by the Veterinary Faculty of Autonomous University of Barcelona (Spain). The vaginal fluid simulant (VFS) was purchased from

Biochemazone (Canada). NovaSyn TGR resin, 9-fluorenyl-methoxycarbonyl (Fmoc) protected D-amino acids and 5(6)-carboxy-tetramethyl-rhodamine were purchased from Novabiochem (Merck). Peptide-synthesis-grade dimethylformamide (DMF) and trifluroacetic acid (TFA) were from Scharlau (Spain). HPLC-grade acetonitrile was supplied from Fisher Scientific (UK). Acetic acid and diethyl ether were acquired from Panreac (Germany). The coupling reagent, 2-(1*H*-7-azabenzotriazole-1-yl)-1,1,3,3-tetramethyluronium hexafluorophosphate methanaminium (HATU), was purchased from RayBiotech (USA). Diisopropylethylamine (DIPEA), *N*,*N*′-diisopropylcarbodiimide (DIPCDI), 1-hydroxybenzotriazole (HOBt), piperidine, triisopropylsilane (TIS), and 2-mercaptoethanol were supplied from Sigma-Aldrich (Merck, Germany).

2.2. Preparation of the hydrogel

2.2.1. Synthesis of RE-E1P47. The retro-enantiomer analog of E1P47 (RE-E1P47) was manually synthesized by solid-phase peptide synthesis (SPPS) as a C-terminal carboxamide following a 9-fluorenyl-methoxycarbonyl (Fmoc)/*tert*-butyl (*t*Bu) chemical strategy. Fmoc-D-amino acids were used throughout the synthesis that were activated with HATU and DIPEA using 3 molar excesses. The synthesis, purification and characterization of the peptide were reported previously.[25]

2.2.2. Fluorescent labelling of RE-E1P47. RE-E1P47 was labelled at the N-terminus with 5(6)-carboxy-tetramethyl-rhodamine (Rho) in the solid phase (see Fig. 1). A fraction of the peptidyl-resin was treated with Rho previously activated with DIPCDI and HOBt. The coupling reaction was carried out overnight with a threefold excess of the reagents.

The peptide was concomitantly side chain deprotected and cleaved from the resin by treatment with a mixture of 94% (v/v) TFA, 1% (v/v) TIS, 2.5% (v/v) 2-mercaptoethanol and 2.5% (v/v) water for 3 h with occasional agitation at room temperature. The TFA was evaporated under a N_2 flow. Diethyl ether was added to precipitate the crude peptide, which was isolated by centrifugation. The solid was dissolved in 10% acetic acid in water and lyophilized.

The RE-E1P47-Rho peptide was purified by RP-HPLC (Waters 1525P, Milford, MA, USA) in a ZORBAX Eclipse XD8-C8 semi-preparative column (5 μm, 9.4 × 250 mm, Agilent Technologies, Santa Clara, CA, USA) at a flow of 10 mL min^{-1}. The purified peptide was characterized by analytical RP-HPLC and ESI-MS (Fig. S1, ESI†) on a Waters ACQUITY Arc multi-dimensional liquid chromatograph (MDLC) (Waters Corporation, Mildford, CT, USA) coupled to a photo diode array (Waters PDA 2998) detector, an evaporative light-scattering (Waters ELS 2424) detector and a single quadrupol mass detector (Waters SQ Detector 2). Analytical RP-HPLC was performed on a ZORBAX® RR Extent C18 column (2.1 × 50 mm, particle size 3.5 μm) with a gradient of 95–5% A in B over 5 min at a flow rate of 0.7 mL min^{-1} using 0.05% formic acid in water (A) and 0.05% formic acid in acetonitrile (B) as an eluting system.

2.2.3. Hydrogel formulation. HG was prepared following the film hydration method, according to the literature.[20,23,28,29] In summary, HSPC and DOTAP were solubilized with chloroform in a round bottom flask and slowly evaporated with a rota-evaporation system to obtain a lipid film. Afterwards, the film was hydrated with an aqueous solution of peptide using an ultrasound bath at 25 °C. Then, a temperature cycle was performed in a closed vial: first, it was frozen at −20 °C for 3 h, then heated at 70 °C for 10 min, and finally, the solution was left to cool at 5 °C in the fridge to achieve gelation. Gelation was confirmed by the absence of gravitational flow when the test tubes containing the HGs were inverted, the so-called ''inversion test''.

Different HG were prepared loaded with different active molecules. For characterization studies and *ex vivo* mucosa application (Sections 2.3.1–2.3.3, and 2.4), formulas A and B were prepared with the peptide RE-E1P47 covalently bonded with rhodamine (RE-E1P47-Rho). For the efficacy tests (Section 2.5), formulas C and D were used loaded with RE-E1P47. For the

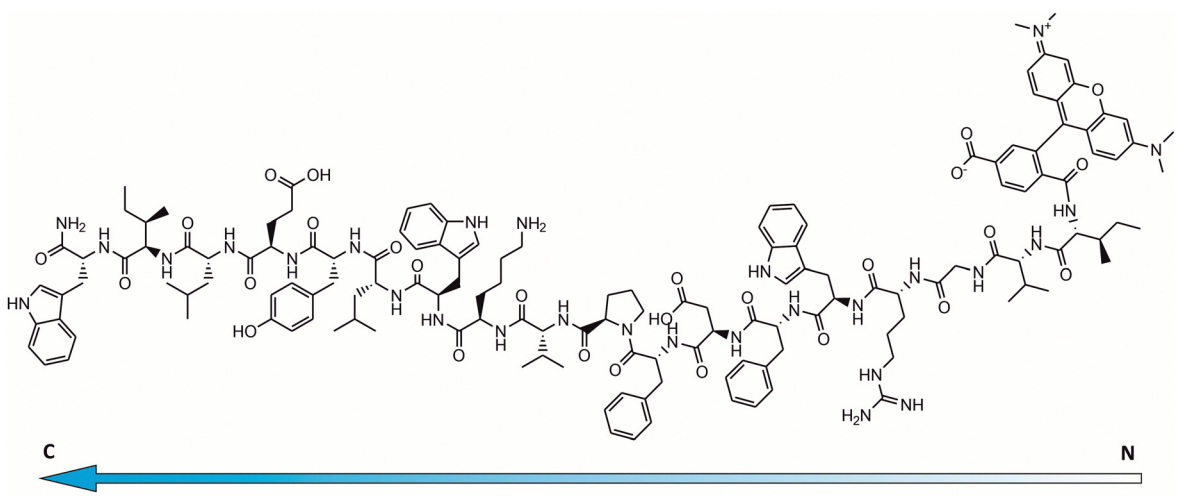

Fig. 1 Primary structure of RE-E1P47-Rho. Software ChemDraw Professional 16 was used.

Table 1 Composition of the hydrogel and control solution with the RE-E1P47-Rho and RE-E1P47

Experiments	Characterization and permeation	Characterization and permeation	VIH efficacy	VIH efficacy	Diffusion	Diffusion
Systems	A Aqueous solution RE-E1P47-Rho	B HG RE-E1P47-Rho	C Aqueous solution RE-E1P47	D HG RE-E1P47	E HG Nile red	F HG Methylene blue
Total	*2000 mg*	*2000 mg*	*2000 mg*	*2000 mg*	*2000 mg*	*2000 mg*
Water	1999.5	1899.5	1999.5	1899.5	1899.8	1900
HSPC	—	95.7	—	95.7	95.7	95.7
DOTAP	—	4.3	—	4.3	4.3	4.3
RE-E1P47-Rho	0.5	0.5	—	—	—	—
RE-E1P47	—	—	0.5	0.5	—	—
Nile red	—	—	—	—	0.2	—
Methylene blue	—	—	—	—	—	0.02

diffusion experiment (Section 2.3.4) systems E and F were used. The final composition of each system is detailed in Table 1.

The different changes in temperature for HG formulation did not alter the stability of the peptide. Previous experiments showed that the peptide remained stable after 10 minutes at 70 °C with no detectable degradation, which is the required temperature for the gelation process of the lipidic HG.

2.3. Characterization

2.3.1. Hydrogel microstructure. HG and water microstructures with the peptide were observed with a High-Speed and Super Resolution Dragonfly 505 (ANDOR) Confocal Microscope System (Oxford Instruments, UK). A CF40-confocal spinning disk large pinhole was used and an oil immersion objective 100×/1.49. Light source excitation was at 561 nm and excitation filter at 594 nm. Images were analyzed with the software Imaris Viewer 9.9.0. (Oxford Instruments, UK).

2.3.2. Molecular interaction analysis. Infrared spectra were obtained using a 360-FTIR spectrophotometer Nicolet Avatar (Nicolet Instruments, Inc., Madison, WI) equipped with an attenuated total reflection (ATR) accessory that used a ZnSe crystal with an angle of incidence of 45° in a horizontal orientation. To collect the sample, all materials were placed onto the crystal, taking care that no bubble air was trapped. All spectra were obtained from an average of 32 scans collected with 2 cm^{-1} resolution over the 4000–500 cm^{-1} region, performed at 25 °C. Three spectra for each material were acquired. Acquisition data and analysis were made with the support of OMNIC software, and an ATR correction was applied to each sample mean.

2.3.3. X-ray scattering: small (SAXS) and wide angle (WAXS). SAXS and WAXS measurements were carried out using a SAXS/WAXS S3-MICRO (Hecus X-ray Systems GmbH, Graz, Austria) coupled to a GENIX-Fox 3D X-ray source (Xenocs) with a wavelength corresponding to the CuKα line (1.542 Å) from the SAXS/WAXS service of the Institute of Advanced Chemistry of Catalonia. The linear detector used was a PSD 50 M (Hecus, Graz, Austria), and the temperature control (precision ± 0.1 °C) was performed *via* a Peltier TCCS-3 (Hecus, Graz, Austria). All samples were introduced into a glass capillary of 2 mm at 25 °C. SAXS and WAXS measurements were carried out with sample-to-detector distances of 268 mm and 282 mm, respectively. The scattering intensity I (in arbitrary units) was measured as a function of the scattering vector q resulting from a photon of wavelength λ scattering off the sample at an angle 2θ, with eqn (1).

$$q = \frac{4\pi \sin\theta}{\lambda} \quad (1)$$

Finally, the Bragg's distance was calculated with eqn (2).

$$d_{\text{Bragg}} = \frac{n2\pi}{q} \quad (2)$$

In a lamellar structure, the various peaks are located at equidistant positions, and Q_n in eqn (3) represents the position of the nth-order reflection.[30]

$$Q_n = \frac{2\pi n}{d} \quad (3)$$

Origin 9.6 (2019) software was used for data analysis and acquisition of q values.

2.3.4. Diffusion studies with vaginal fluid simulant. When a topical system is applied to the vaginal mucosa, the first barrier encountered is the vaginal fluid, where the system might dilute and transfer part of the encapsulated active ingredient. These qualitative diffusion studies investigated the potential interaction of the HG with a VFS to evaluate whether the HG might dilute, interact and diffuse with the vaginal fluid, or undergo structural disruption. To evaluate this, two HG were formulated with two different fluorophores: a HG containing 10 ppm of Methylene blue (MB) and a HG containing 100 ppm of Nile red (NR) (see Table 1, systems E and F). For this study, a homemade device was designed using a glass capillary tube, 5 mm external diameter and 0.5 mm wall thickness, cut into two sections. The HG was introduced into the lower capillary, while the VFS was placed in the upper tube. The two capillaries were joined and sealed with high vacuum grease to create a liquid–gel interface, enabling the observation of fluorophore diffusion from one medium to the other. Photographs were taken at intervals from the initial formation of the interface (time 0) up to 24 hours. These images were captured using a CANON Power Shot S90 Image Stabilizer (Canon Inc, Japan) under fixed photography conditions with a constant sample-to-camera distance and fixed illumination conditions. All images were processed with ImageJ software. Finally, a graphic representing a color intensity curve as a

function of time and distance along the capillary could be drawn. Insights were obtained regarding the behavior of the HG in contact with a VFS, including whether its structure is disrupted or if part of the active ingredient is released into the fluid.

2.4. *Ex vivo* permeation studies with mucosal tissue

2.4.1. Preparation of mucosa samples. Ovine vagina tissue was obtained from the Veterinary Faculty of Autonomous University of Barcelona (Spain). The vagina was removed from the sheep minutes after the animal was sacrificed for medical experimentation. The protocols used were approved by the Ethical Commission of Animal and Human Experimentation (Spanish Government) under the auspices of the Ethical Commission of the Autonomous University of Barcelona. A PBS solution was prepared dissolving one tablet in 200 mL of Milli-Q water (0.01 M Phosphate buffer, 0.0027 M KCl, 0.137 M NaCl), and the entire tissue was preserved in this solution at 8 °C for 18–24 hours until use.

For mucosa preparation, the tissue was cut in 1.5 cm × 1.5 cm pieces, and then 30 mg of sample were applied onto the surface of the mucosa pieces with an area of application of 0.5 cm^2. After 16 h incubation at 37 °C in a wet environment, the excess of material on the surface was removed gently with filter paper and the mucosa was washed with 10 μL of water.

2.4.2. Fluorescence microscopy of transversal mucosa sections. After mucosa incubation and washing, the mucosa treated area was cut into 0.5 cm × 0.5 cm sections and covered with cutting temperature compound (OCT). Afterward, they were frozen in liquid nitrogen before cutting into transverse 25 μm thick sections with a Cryostat CM3050 (Leica Biosystems Nussloch, Germany). Skin sections were then placed onto microscope slides. Next, staining was applied to mucosal slices to recognize the mucosal surface area in the micrographs. A solution of 1 μL of Hoechst solution and 1 μL Wheat Germ Agglutinin (WGA) Alexa Fluor 488 in 1 mL of MilliQ water was applied on the mucosal sections, which were left for 20 min protected from light. Afterwards, the stained solution was removed, and the mucosa slices were washed with MilliQ water. Subsequently, the mucosal slides were covered with FluorSaveTM Reagent and sealed. They were observed with a high-speed fluorescence microscope Leica Thunder. Mosaic images were captured using a HC PL APO 40×/0.95 DRY objective. The exposure time was set to 75 ms, with a 594 nm excitation filter used for peptide red-fluorescence, a 440 nm excitation filter for nucleus blue-fluorescence, and a 519 nm excitation filter for polysaccharide green-fluorescence. Image analysis was performed using ImageJ software.

Data on fluorescence intensity were obtained from all the micrographs within a mucosal surface area extending up to approximately 150 μm in depth. The background signal was obtained from the empty area next to the mucosal surface for each micrograph. Then, all data were treated according to the statistical analysis. To compare images of different treated samples, brightness and contrast were adjusted uniformly across all fluorescent images for consistency in comparison.

Three straight lines for each micrograph were taken to obtain data on the length of the permeability micrographs within a mucosal surface area extending up to approximately 150 μm in depth. To compare the permeation between the different treated samples, data were treated according to statistical analysis.

2.4.3. Fluorescence confocal microscopy of full-mucosa tissue. To observe the full-skin mucosa tissue, the treated mucosa pieces were cut into 0.5 cm × 0.5 cm sections. Subsequently, the mucosal surface was placed upside down on a cover slip and was observed with a high-speed and super resolution Dragonfly 505 (ANDOR) Confocal Microscope System (Oxford Instruments, UK). A CF40-confocal spinning disk with a large pinole and a multi-inversion objective 10×/0.5 with water immersion were used. The exposure time was set to 150 ms and the *Z*-axis range was approximately between 90–100 μm. Confocal images were captured at intervals of 2.34 μm along the *Z*-axis. The excitation light source was set at 561 nm with an excitation filter at 594 nm. Images analysis was performed using ImageJ software. Fluorescence intensity data were collected from the bright areas of each confocal plane, and the background signal was obtained from areas with lower intensity for each micrograph. Then, all data were treated according to the statistical analysis. To compare images of different treated samples, brightness and contrast were adjusted uniformly across all fluorescent images for consistency in comparison.

2.5. Efficacy test against *ex vivo* HIV infection of the human cervicovaginal mucosa explant tissue model

Cervical tissue samples were obtained from women undergoing non-neoplastic hysterectomies at the Vall d'Hebron University Hospital (HUVH, Barcelona, Spain). Participants in this study signed a written informed consent before sample collection and a Comitè d'Ètica d'Investigació Clínica (Institutional Review Board numbers PR (IR) 294/2017) approved all the study protocols. Samples were processed immediately after surgery, following the protocol described in ref. 31. Briefly, after resecting stromal tissue, 2 mm^2 deep mucosal fragments of 20–30 mm^2 in length were incorporated into a 24-well transwell plate, following established protocols by Abner *et al.*[32] and Ouattara *et al.*,[33] to achieve mucosal polarization.

Four experimental conditions were evaluated per individual tissue: two controls—one treated with PBS and another with the hydrogel control (HG control) base without the peptide—and two test samples, one containing the aqueous solution of the anti-HIV peptide RE-E1P47 and the other incorporating the peptide within the HG base (refer to Table 1, systems C and D). A defined volume (15 μL) of each formulation was applied onto the mucosal surface, followed by incubation at 37 °C with 5% CO_2 for 16 hours. After incubation, tissues were washed twice with PBS and subsequently infected with HIV_{BaL} (10 μL, $TCID_{50}$ 156 250, kindly provided by Dr Julia G. Prado), as performed before.[34] Mucosal explants were maintained for 5 days with Dulbecco's modified Eagle's medium (DMEM – Fisher Scientific; #41966029) supplemented with 20% Fetal Bovine Serum (FBS – Life Technologies; #A5256701) with one media change on day 3, after which they were digested as we have previously described.[31,34]

After digestion, the resulting cell suspension was washed twice with PBS and stained with live/dead aqua (Invitrogen, #L34966; 1 : 250) to distinguish viable from non-viable cells. Surface staining was performed using the following antibodies: CD45 (AF700, clone HI30, Biolegend, #304024; 1 : 100), CD3 (BV650, clone UCHT1, BD Biosciences, #563852; 1 : 40), and CD8 (APC, clone RPA-T8, BD Biosciences, #555369; 1 : 40). To evaluate HIV infection, cells were fixed with Fixation Medium A (Thermo Fisher Scientific, #GAS001S100) and permeabilized using Permeabilization Medium B (Thermo Fisher Scientific, #GAS002S100), following the manufacturer's protocol. Intracellular staining for HIV p24 was performed with anti-p24 antibody (PE, clone KC57-RD1, Beckman Coulter, #6604667; 1 : 200), as described by Cantero-Pérez *et al.*[34]

Fluorescence minus one (FMO) controls were employed to delineate gating strategies in the different conditions. Samples were acquired in the Aurora full-spectrum flow cytometer (Cytek Biosciences) at the Flow Cytometry Platform from Vall d'Hebron Institut de Recerca (VHIR) and analyzed with FlowJo vX.0.7 software (TreeStar).

Considering that the metabolic stability of this peptide was previously reported,[25] demonstrating that RE-E1P47 is not degraded by proteases and retains more than 90% of its efficacy after 24 hours, along with an efficacy assay that lasted 15 days in mucosal explants[25] under continuous peptide application (mimicking sustained exposure) or without peptide application (mimicking pulse exposure) at different concentrations, we considered that under similar experimental conditions—such as those used for maintaining mucosal explants in DMEM supplemented with 20% Fetal Bovine Serum—the peptide remained stable throughout this *ex vivo* experiment.

2.6. Statistical analysis

For the *ex vivo* permeation studies, to compare the intensity values obtained with fluorescence microscopy (Sections 3.2.1 and 3.2.2), intensity data were analyzed with ImageJ. The data distribution was asymmetrical, so the Napierian logarithm (ln) from the intensity values was calculated to transform all data into a symmetrical distribution. Box plots of the ln transformation were represented with Origin 2019.

For fluorescence microscopy of transversal mucosa sections (Section 3.2.1), data on fluorescence intensity were obtained from all the micrographs within a mucosal surface area extending up to approximately 150 μm in depth. The background signal was obtained from the empty area next to the mucosal surface for each micrograph. To compare permeation differences between each material, data were analyzed with Brown–Forsythe and Welch ANOVA test. Then, to compare the depth permeation of the peptide in the mucosa transversal sections, three straight lines for each micrograph were taken from all micrographs. To compare the depth permeation between the different treated samples, an Unpaired *t*-test with Welch's correction was performed. Statistical significance was determined by *p*-values < 0.05. For fluorescence confocal microscopy of full-skin tissue (Section 3.2.2), confocal images were captured at intervals of 2.34 μm along the *Z*-axis. Fluorescence intensity data were collected from the bright areas of each confocal plane, and the background signal was obtained from areas with lower intensity for each micrograph. Then, to determine the permeation of the peptide between materials, the confocal planes with the maximum intensity were processed with ImageJ software and an Unpaired *t*-test with Welch's correction was performed. The depth permeation was calculated from these maximum intensity confocal planes (taking into account the 2.34 μm intervals along the *Z*-axis). An Unpaired *t*-test with Welch's correction was performed to compare both populations. Statistical significance was determined by *p*-values < 0.05. All statistical analysis was performed with GraphPad Prism 9.

For the efficacy *ex vivo* assays described in Section 3.3, data were analyzed using a non-parametric Friedman ANOVA test with Dunn's correction for multiple comparisons, as well as the Wilcoxon matched-pairs signed rank test for paired data. All values in the graphs are expressed as the median and the range or the interquartile range. Statistical significance was determined using GraphPad Prism 9, and a P value < 0.05 was considered significant.

3. Results and discussion

3.1. Characterization

3.1.1. Microstructural study. The microstructure of the aqueous solution and the HG incorporating the peptide RE-E1P47-Rho (systems A and B from Table 1) was visualized using fluorescence microscopy. In Fig. 2, images of the HG (A) and water solution (B) both with the fluorescent peptide RE-E1P47-Rho are presented. The HG structure (Fig. 2A) shows round, highly packed structures between 5 and 20 μm in diameter, corresponding to lipid vesicles. Many of these vesicles appear to be multilamellar and extend throughout the aqueous phase forming the gel. Since the fluorescence is due to the Rhodamine covalently bonded to the peptide, the peptide is localized within the lipid bilayers of the vesicles comprising the HG structure. The structure of this HG was previously studied in our research group.[20–23] CryoTEM studies showed that HG is formed by small and large vesicles ranging from 30 to 150 nm, which form branched aggregates,[22] while larger vesicles (5 to 20 μm in diameter) were imaged by confocal microscopy.[20,22,23] Our previous studies demonstrated the multilamellarity of these HG structures using SAXS and confocal microscopy.[20,22] Results presented in this study, in which the HG incorporates a lipophilic peptide clearly show a material with a similar structure. The HG exhibits large multilamellar vesicles and regions where lipid structures are clustered in vesicles (fitting with those previous studies). According to Gomara *et al.*,[25] the peptide RE-E1P47 has the affinity to assemble into cell lipid bilayers. Fig. 2A shows the peptide localization within the lipid bilayers of the HG in this case (in red color) correlating with the results of Gomara *et al.*. Conversely, the peptide forms microscopic aggregates when it is dispersed in water (Fig. 2B) due to the lipophilicity of the peptide.

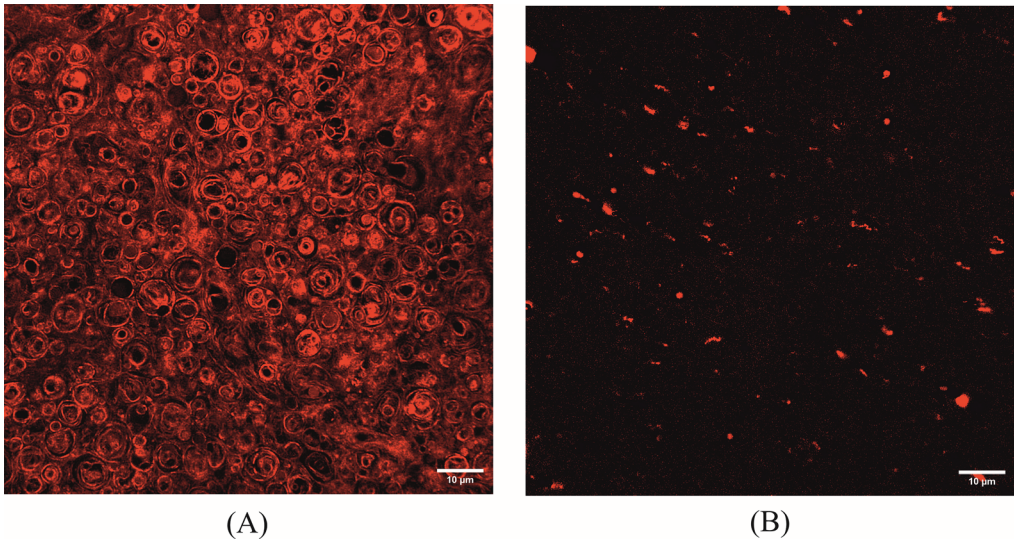

Fig. 2 Fluorescence micrographs of (A) HG RE-E1P47-Rho and (B) water solution of RE-E1P47-Rho. Reference bar corresponds to 10 μm.

3.1.2. Molecular interaction analysis. Attenuated total reflectance-Fourier transform infrared (ATR-FTIR) spectroscopy was used to identify functional groups present in the samples, reporting information about the interactions of the peptide RE-E1P47-Rho with the different systems. In Fig. 3, ATR FT-IR spectra from the aqueous solution and the HG loaded with RE-E1P47-Rho are presented. Both samples present the principal vibrations in 3400 and 1650 cm^{-1}. Additionally, the HG sample presents two small peaks at 2850 cm^{-1} and 2920 cm^{-1}. Moreover, a vibration is detected at 2360 cm^{-1} in all measurements attributed to CO_2. This signal is not associated with any molecular vibration of the samples.[20,35,36]

The absorption bands at 3400 cm^{-1} and 1650 cm^{-1} are commonly associated with the O–H stretching and H–O–H scissors bending from water.[37] These bands are clearly observed in both samples due to their high-water content, as can be observed in Table 1 (systems A and B). The CH_2 symmetrical and asymmetrical stretches (2850–2920 cm^{-1}) appear only in the HG sample. This range of wavelengths corresponds to aliphatic chain stretching from the 5% lipid content regarding HSPC and DOTAP (see Table 1). These peaks overlap with the broad band at 3400 cm^{-1}.[20,35] The lipids forming the microstructure of the HG contain HSPC and DOTAP. Both have C═O functional groups. However, the peak corresponding to the C═O stretch of the ester carbonyl functional group is not seen in this spectrum. As described in the literature, according to Alinaghi *et al.*[38] and Campbell *et al.*,[39] vibrations of ester C═O bonds depend on the chemical structure of the polar head from the lipid blend. In our case, the presence of the positive charge due to the DOTAP cationic lipid would explain a possible shift of the peak from 1743 to 1647 cm^{-1}. In this case, the C═O peak from the HG may be overlapped with the 1650 cm^{-1} peak from water.[20] Furthermore, our previous studies[20] reported the ATR-FTIR spectra of this very same lipid HG without the peptide, and the spectra of this

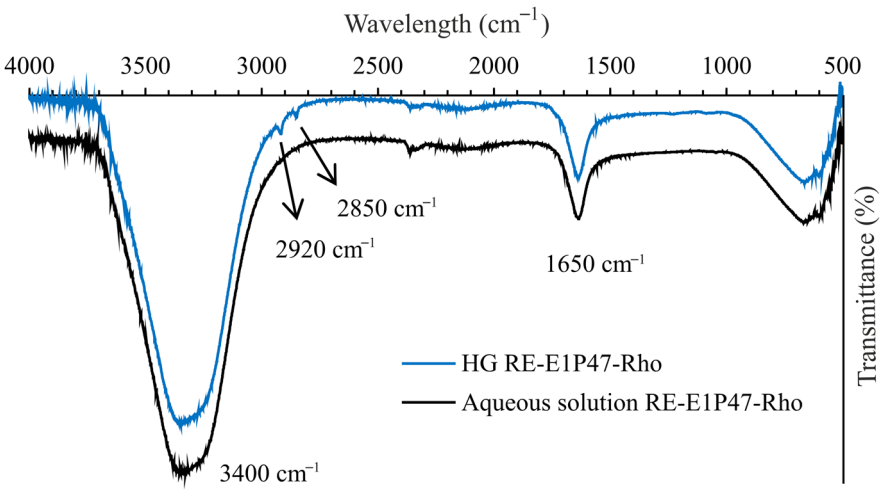

Fig. 3 ATR-FTIR spectra of the aqueous solution of RE-E1P47-Rho and the HG RE-E1P47-Rho.

study obtained the same results, so it can be said that the incorporation of the peptide into the HG does not alter the microstructure of the gel.

3.1.3. X-Ray scattering: SAXS and WAXS. X-Ray scattering has been used to study the phase behavior and organization of lipids in the vesicles forming the HG to study whether the incorporation of RE-E1P47-Rho may change this organization. Small-angle X-ray scattering (SAXS) provides information about the arrangement of lipid molecules and the crystallinity of the lipid bilayer forming the HG. Alternatively, wide-angle X-ray scattering (WAXS) reports lateral packing organization, providing the distance between neighboring molecules. Fig. 4A and B show SAXS and WAXS profiles of the aqueous solution and the HG loaded with RE-E1P47-Rho.

The structure of the HG without peptide was previously studied in our research group.[20–23] Regarding the HG sample with RE-E1P47-Rho (blue color), the SAXS profile (Fig. 4A) shows a main wide band centered at an approximate q value of 0.10 $Å^{-1}$, followed by two additional lobes at 0.25 $Å^{-1}$ and 0.39 $Å^{-1}$. The shape of this SAXS profile for the HG (Fig. 4A) is characteristic of a scattering pattern associated with uncorrelated bilayers of different vesicle sizes. These q values correspond with those of the HG without the peptide (green color). They were previously identified by Talló *et al.*[22] and corroborated by our previous studies again with the same HG without the peptide.[20,29]

The WAXS plot for HG (Fig. 4B) showed a single broad band centered at q = 1.46 $Å^{-1}$ corresponding to a d-spacing of 4.3 Å between hydrocarbon chains, which is characteristic of a lipid lamellar gel phase organized in a two-dimensional hexagonal lateral packing.[21,22,40] The presence of a single broad band instead of a sharp peak indicates that the chains are less organized but still form this lateral packing.

No reflections were detected in the SAXS/WAXS measurements for the aqueous solution of the peptide. This indicates the lack of an organized structure of this peptide in water. This fact is in accordance with microscopy observations in Section 3.1.1, which showed that the peptide forms aggregates in water.

Our SAXS and WAXS experiments indicate that the incorporation of the peptide in the HG leads to the characteristic structural organization described for this material. The comparison between the reflections of Fig. 4A and B with our previous studies,[20,22] confirms that the HG maintains its original structural organization despite the presence of RE-E1P47 in the lipid bilayer.

3.1.4. Diffusion studies with vaginal fluid simulant. These qualitative diffusion studies investigated the potential interaction of the HG with a VFS to evaluate whether the HG might dilute, interact and diffuse with the vaginal fluid, or undergo structural disruption. Two HG with different fluorophores were used, one with Methylene blue and the other with Nile red (see Table 1, systems E and F).

In Fig. 5A, five representative photographs of the two capillaries junction are shown, where the diffusion interface between the HG 10 ppm MB and VFS was established. The images were taken at different time points, starting from the beginning of the experiment (T0) up to 22 hours. These selected photographs illustrate the diffusion of the fluorophore from the HG (lower blue section) into the VFS (upper section). Fig. 5B presents the corresponding color intensity graph along the capillary. T0 represents this, and all photographs were treated separating the RGB colors. Then, a vertical line was drawn along the capillary, and finally the intensity values of the red RGB intensity was analyzed. The left side of the graph in Fig. 5B represents the intensity of the VFS, transitioning through the interface and ending with the color intensity of the HG. In Fig. 6, the diffusion experiment using NR is represented. Fig. 6A shows five photographs of the assembled device with the interface assembled between the HG NR and the VFS, taken at different times from the start of the experiment (T0) to 22 hours. In this case, the graph in Fig. 6B represents the green channel intensity from the RGB analysis.

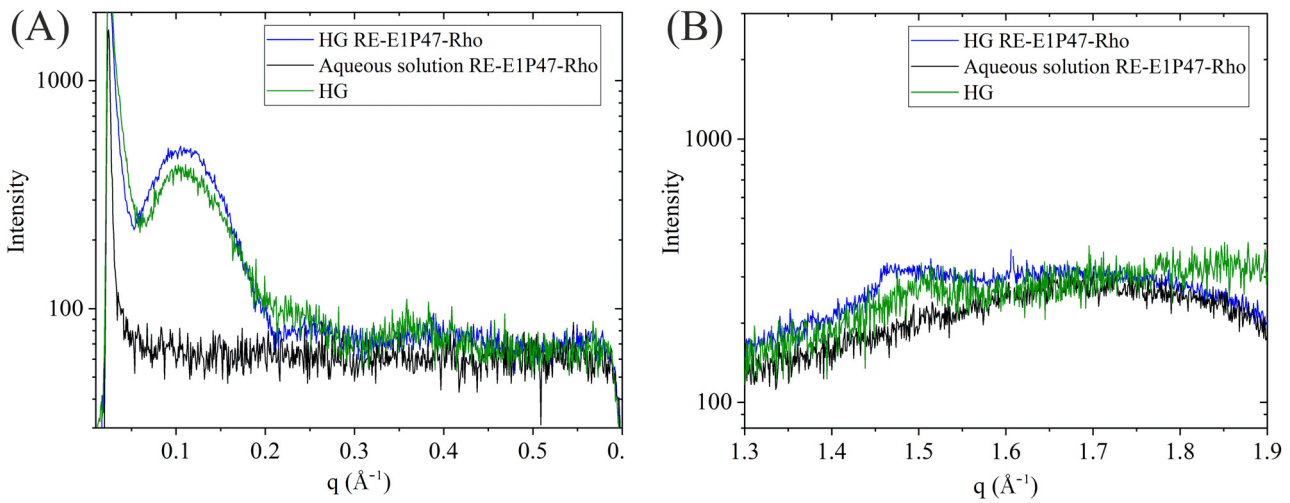

Fig. 4 (A) Small angle X-ray scattering (SAXS) and (B) wide angle X-ray scattering (WAXS) intensity profiles of the aqueous solution and the HG loaded with RE-E1P47-Rho.

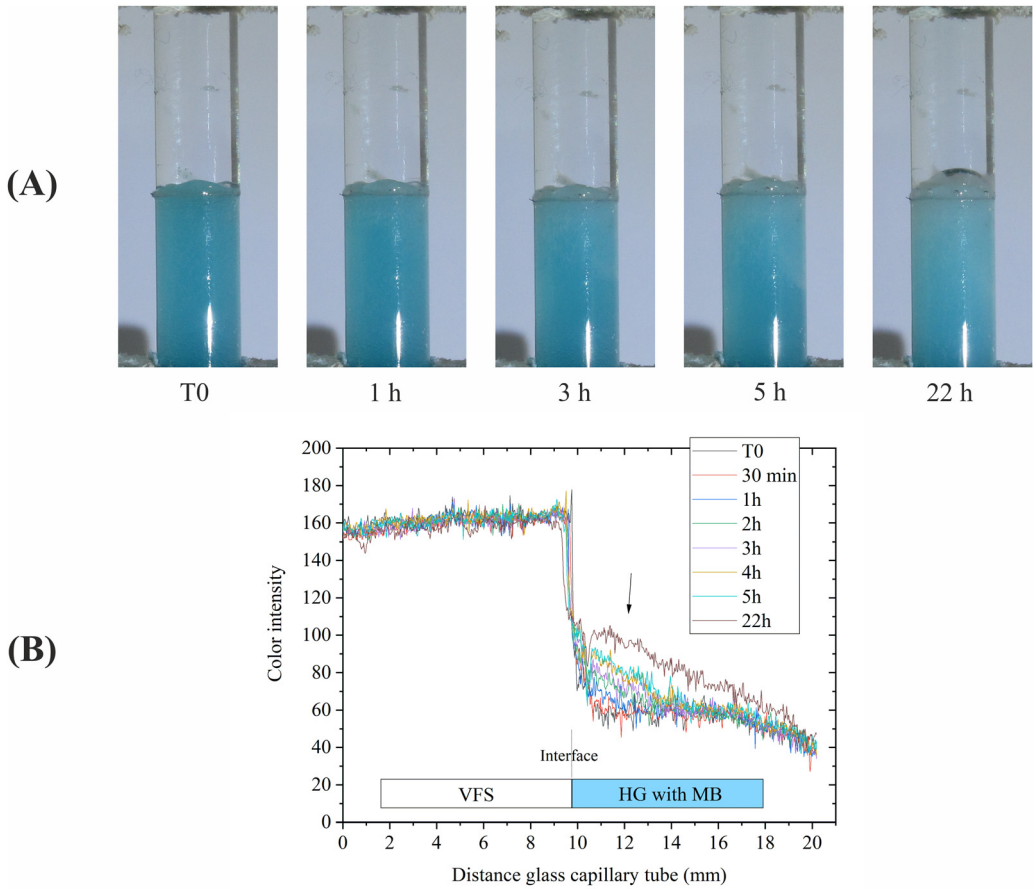

Fig. 5 (A) Capillary tube photos at different times for the diffusion studies with the HG 10 ppm MB *vs.* VFS. (B) Graphic representing the red RGB color intensity of the two sections of the capillary tube from T0 to 22 h.

The results show a very subtle color change in the HG with MB (Fig. 5A). After six hours, the gel becomes slightly whitish at the interface area. This change is also evident in the graph of Fig. 5B (see the arrow), where a shift is observed in the baseline curve of the HG due to the color change. This is hypothesized to be caused by gel hydration, which affects light scattering and results in a subtle color change. However, it cannot be determined if this represents a change in the concentration of the fluorescent molecule within the gel, as the phenomenon is not governed by Beer–Lambert's law. Instead, the color change is likely related solely to an increase of dispersed light caused by hydration. In addition, no sign of release to the aqueous media was observed, agreeing with the above observation. Also, experiments with the same setup using a transparent polymeric gel, did show a sigmoidal profile of color without changes in the blue color tone (no whitening), proportional to concentration and agreeing with a simple diffusion.

For the diffusion experiment with NR, this effect is much less evident, even though the HG is the same. This is likely because the fluorophore is encapsulated in the lipid bilayer rather than being dissolved in water. As a result, the effect of hydration on light scattering is less noticeable.

Furthermore, no diffusion of either molecule (hydrophilic or lipophilic) from the HG into the VFS was observed. Moreover, after 22 hours, a bubble formed at the interface due to imperfect sealing of the capillary tubes. Despite this bubble formation, no diffusion of the molecules was observed. If diffusion had occurred, a color gradient would be visible in Fig. 5A and 6A, and a change in the slope of the VFS baseline curve in Fig. 5B and 6B would be apparent. Instead, a sharp slope change is observed at the interface, where the curve becomes completely vertical. However, a slight swelling of the gel is apparent in both cases, note the small displacement of the vertical part of the curves (the interfaces) to the left (Fig. 5B and 6B). In the latter case, a lump of gel seems to have detached and disappeared from the window of observation due to lower gel density.

In this experiment, the difference in viscosity is much more important for diffusion than density. We calculated the densities of HG according to the weight of the phospholipids, yielding a density 0.04% lower than that of water (0.996 g mL^{-1} *vs.* 1 g mL^{-1}). Visually, this does not produce any noticeable differences in volume. The HG at the interface swells due to the incorporation of water from the VFS into the gel, not because of a significant change in density. At most, there would be a slight shift from 0.996 to 0.998 g mL^{-1}—differences that do not affect diffusion in this experiment. Since the densities of the VFS and the HG are practically the same, without a significant change, it is considered that they do not impact diffusion.

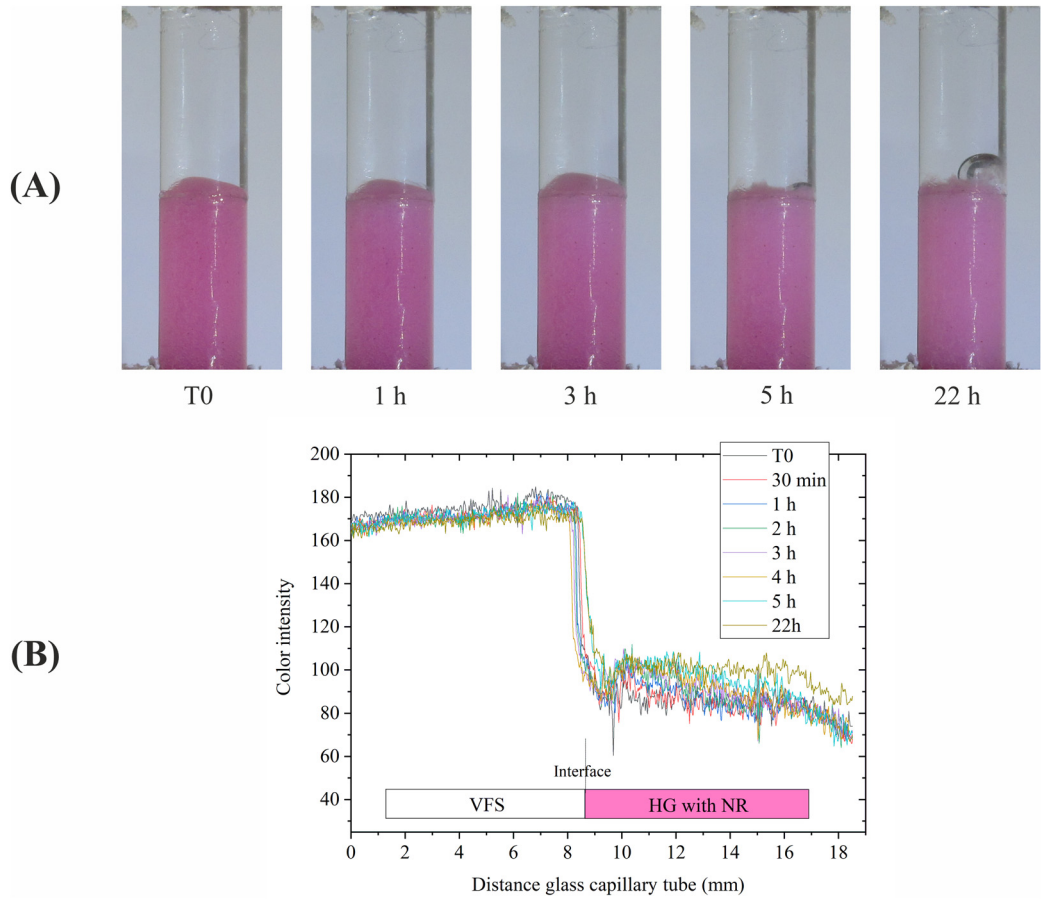

Fig. 6 (A) Capillary tube photos at different times for the diffusion studies with the HG 100 ppm NR *vs.* VFS. (B) Graphic representing the green RGB color intensity of the two sections of the capillary tube from T0 to 22 h.

Our initial hypothesis was that the two molecules would behave differently in terms of diffusion. First, MB, being hydrophilic, is expected to be dissolved in the water both inside and outside the vesicles that form the HG. When the HG encounters the VFS, there would be diffusion of the MB present in the water outside the vesicles into the VFS. However, this does not occur. If the VFS disrupted the HG, we would observe diffusion of the unencapsulated MB. Alhelal *et al.*[41] reported that a HG loaded with solid–liquid nanoparticles exhibited an initial rapid drug release, attributed to the drug located outside the encapsulation, followed by a sustained delayed release. However, the interphase conditions in their experiments differ from those in this study. Regarding NR, this lipophilic molecule is located in the lipid bilayer, similar to the peptide studied in this article. Therefore, diffusion through the VFS would not be expected. Any diffusion observed would likely result from HG rupture and subsequent vesicle release and the NR within. However, no such behavior is observed even after 22 hours.

Finally, the results indicate that the HG does not break down in contact with the VFS, nor does it diffuse as isolated vesicles. The behavior of the HG containing NR can be correlated with the expected behavior of the encapsulated peptide, which is also lipophilic. It can be hypothesized that the HG will have greater affinity for mucosal tissue than for the VFS, facilitating the delivery of the molecule carried by the HG to the tissue. This penetration would be likely promoted by the lipids in the HG and mechanical application in a real topical scenario.

3.2. *In vitro* mucosal skin permeation studies

3.2.1. Fluorescence microscopy of transversal mucosa sections. To study the permeation of the fluorescent peptide RE-E1P47-Rho, three samples were analyzed: control mucosa, mucosa treated with an aqueous solution, and mucosa treated with the HG, both (aqueous solution and HG) loaded with the fluorescent peptide (systems A and B from Table 1). The control mucosa was treated only with water to evaluate the autofluorescence of the tissue section. Sheep vaginal mucosa was used as a model for the human vagina due to similarities in anatomical and microscopic features.[42–44] Additionally, previous studies have demonstrated that sheep mucosa serves as an effective *ex vivo* model for permeation barrier experiments with various materials.[26,44,45]

Fig. 7 shows microscope images of 25 μm mucosa slices treated with the different samples: (1) control, (2) an aqueous solution of RE-E1P47-Rho, and (3) the HG loaded with RE-E1P47-Rho. Images were captured using a Leica Thunder microscope, with different filters applied: a 594 nm excitation filter for the peptide's red fluorescence, a 440 nm excitation

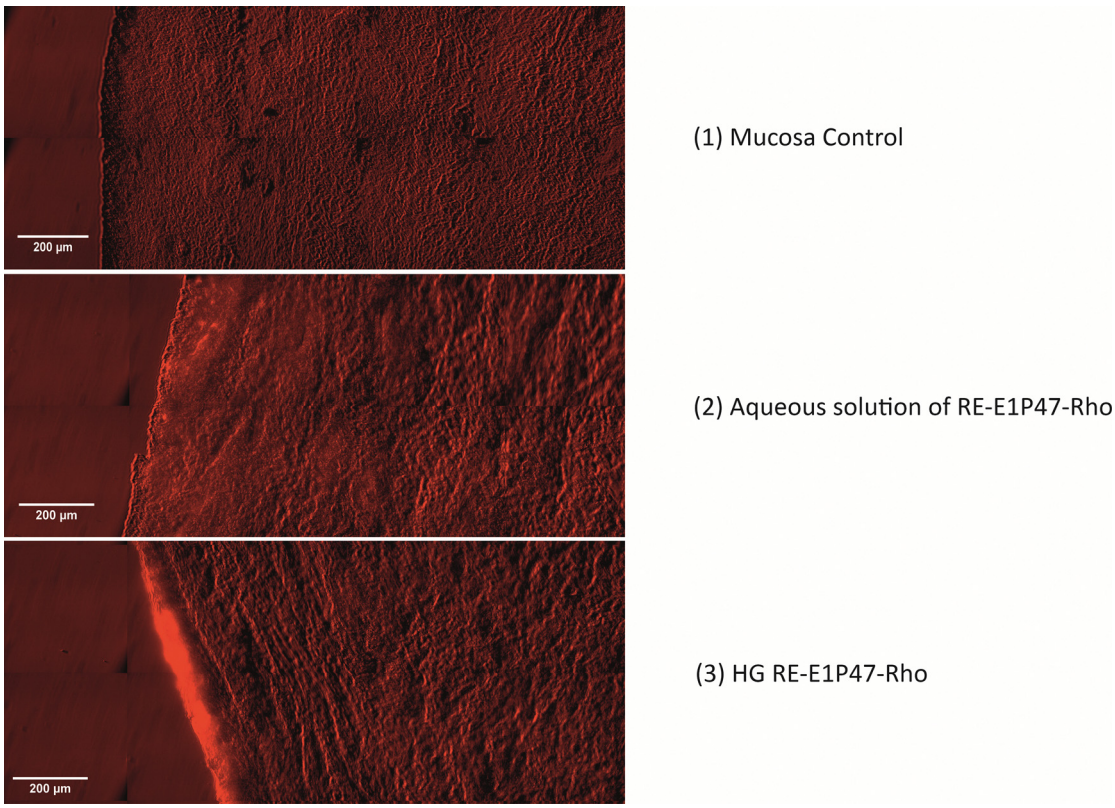

Fig. 7 Micrographs were obtained from skin slices treated with (1) the control, (2) an aqueous solution of RE-E1P47-Rho and (3) HG loaded with RE-E1P47-Rho. The reference bar corresponds to 200 μm. These images were captured with a 594 nm excitation filter to detect the red fluorescence of the peptide. Qualitative analysis was conducted by comparing the intensity values from each sample. Images were processed using ImageJ, with intensity values ranging from 500 to 2000 (on a scale of 0 to 65 535).

filter for blue fluorescence to visualize the cell nuclei, and a 519 nm excitation filter for polysaccharide green fluorescence. Image analysis was conducted using ImageJ software. Despite the fact that blue and green fluorescence images are not shown, they were used to identify the mucosa surface area for peptide localization study, where intensity values were measured afterwards with the red fluorescence filter.

Fig. 8A shows the box plot of the logarithmic intensity values obtained from all the micrographs within a mucosal surface area extending up to approximately 150 μm in depth. This visualization allows for the comparison of the relative quantification of peptide permeation when applied with the HG *versus* the aqueous solution and the control. In both Fig. 7 and 8A, control values are included to assess the mucosa's autofluorescence when treated with water, providing a baseline for comparing the intensities of the peptide-loaded samples. Fig. 8B illustrates the different penetration distances at which fluorescent areas, corresponding to peptide permeation, were observed in the various micrographs. Three distance values were recorded for each micrograph. Since no fluorescent areas were detected in the control sections, no distance values are included for the control, which is therefore considered to have a permeation distance of zero. The raw data supporting Fig. 8A and B are provided in the ESI,† Tables S1 and S2, respectively.

Peptide permeation results (Fig. 8A) indicate significant differences among all three samples. For the control sample, autofluorescence was measured to serve as a baseline for comparison, confirming that peptide concentrations in the treated samples were sufficient to distinguish them from control fluorescence. The results show that the relative amount of peptide retained on the mucosal surface was higher when applied with the HG than with the aqueous solution. As seen in Fig. 7 and 8A, greater fluorescence intensity was observed on the mucosal surface, indicating a higher peptide content. Statistical analyses can be found in the ESI,† Tables S3 and S4. Fig. 8B illustrates the depth of peptide permeation into the mucosa when applied using the HG and the aqueous solution. Our findings indicate that the peptide penetrated more deeply with the aqueous solution ($\sim$105 μm) than the HG ($\sim$75 μm); however, as shown in Fig. 8A, the amount of peptide retained in the mucosa was lower in this case. The intended application aims to achieve high peptide retention on the surface rather than deep tissue permeation. Results show that the HG allows for a greater quantity of peptide to be introduced and retained on the mucosal surface.

The composition and properties of the HG play a crucial role in its interaction with mucosal tissue and in the permeation of encapsulated agents. The HG formulation, based on phospholipids forming bilayers, promotes both adherence and

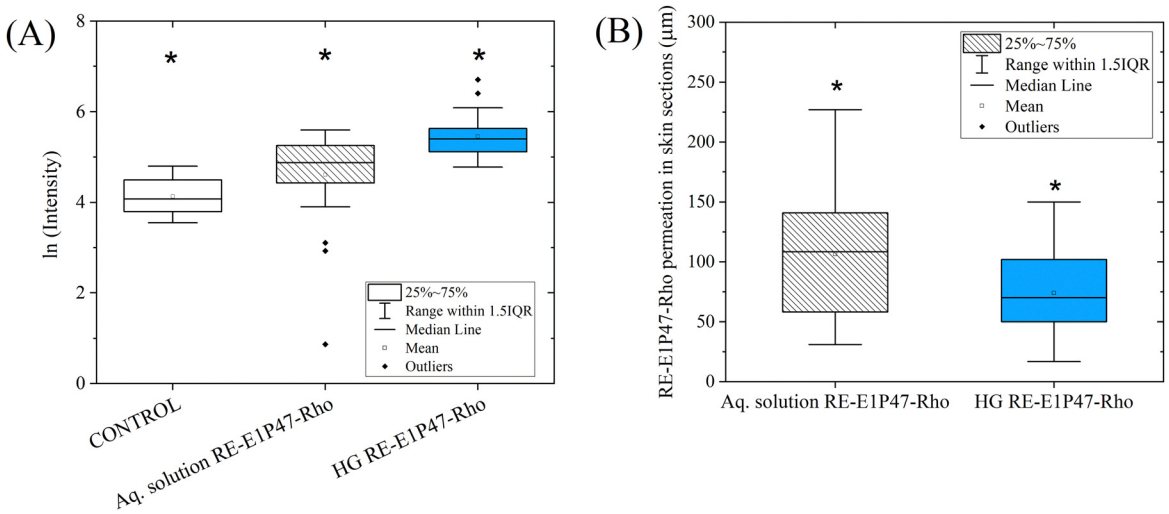

Fig. 8 (A) Box plot representation of the fluorescence microscopy results showing RE-E1P47-Rho permeation using the aqueous solution and the HG (systems A and B in Table 1). All results showed significant differences. (B) Box plot representing the permeation depths (in µm) of RE-E1P47-Rho, based on the material applied onto the mucosa. Since no fluorescent areas were detected in the control sections, no distance values are included for the control, which is therefore considered to have a permeation distance of zero.

penetration into the mucosal surface, an effect enhanced by the electrostatic and hydrophobic interactions of its components. Specifically, DOTAP, a cationic phospholipid included in the HG, provides a mild positive charge to the system, which facilitates interaction with the negatively charged glycoproteins in the superficial layers of mucosal tissue.[10] It could be hypothesized that these glycoproteins promote electrostatic, hydrophobic, and hydrogen bonding interactions with exogenous agents, further supporting the adhesion of the HG. The peptide encapsulation within the HG lipid bilayers also ensures that the peptide remains within the lipid matrix, which may help improve its stability and its delivery localized effect on the mucosal surface.

Previous studies[21,24] have explored the permeation behavior of hydrophilic molecules encapsulated in HG through skin application, finding that the lipid matrix of the HG remains localized within different skin layers. Talló *et al.* reported that the lipid matrix tends to remain in the upper part of the stratum corneum of the skin, without penetrating to the epidermis.[21] Meanwhile, our previous studies demonstrated that when a hydrophilic molecule is incorporated into the HG and applied to the skin, it tends to be retained in the upper layers of the skin.[24]

This study applies the HG to mucosal tissue, which, unlike the skin, lacks a keratinized layer (stratum corneum). Therefore, the HG is directly applied to the upper layer of the vaginal mucosa, a non-keratinized, multi-layered squamous epithelium.[2] Due to the absence of keratinization, the lipids in the HG are expected to interact more directly with the superficial mucosal cells, aiding in the peptide's delivery. As the peptide is a large molecule, it may become retained within the superficial cells of the mucosa and is unlikely to permeate into deeper layers, as it cannot easily pass through. According to the literature,[4,46,47] generally larger molecules have a smaller diffusion permeation than small molecules. This localized retention within the non-keratinized epithelium suggests that the HG could effectively deliver the peptide to targeted areas on the mucosal surface. When dispersed in water, the peptide, which is inherently lipophilic, tends to form aggregates, as shown in Fig. 2B, which hinders its ability to cross the mucosal barrier independently.

3.2.2. Confocal fluorescence microscopy of full-mucosa tissue. In this section, confocal fluorescence microscopy is used to study the permeation and localization of the peptide within the epithelial cells of the mucosa, allowing us to observe its distribution within the cells. Additionally, the relative quantification of the peptide in the mucosa and its permeation depth are analyzed, as in the previous section. Three samples were examined: control mucosa, mucosa treated with an aqueous solution, and mucosa treated with the HG, both loaded with the fluorescent peptide. The control mucosa was treated only with water to evaluate the tissue's autofluorescence. To visualize the mucosal surface, the tissue was placed upside down on a cover slip, and confocal *Z*-planes were taken from the surface downwards until no fluorescence was detected. Since no fluorescence was observed in the control samples, they were assigned a value of zero autofluorescence.

Fig. 9 displays representative confocal images of the *Z*-plane with the highest fluorescence intensity for (A) the aqueous solution of RE-E1P47-Rho and (B) the HG loaded with RE-E1P47-Rho. The images were captured using a high-speed super-resolution Dragonfly 505 Confocal Microscope System (ANDOR, Oxford Instruments, UK). Confocal *Z*-plane images were acquired at 2.34 µm intervals along the *Z*-axis. The images were processed with ImageJ software using the Fire filter. The intensity scale (see Fig. 9) indicates that the yellow color represents higher fluorescence intensity, transitioning through purple and ending with blue for the lowest intensity. This gradation allows us to visualize the concentration of the

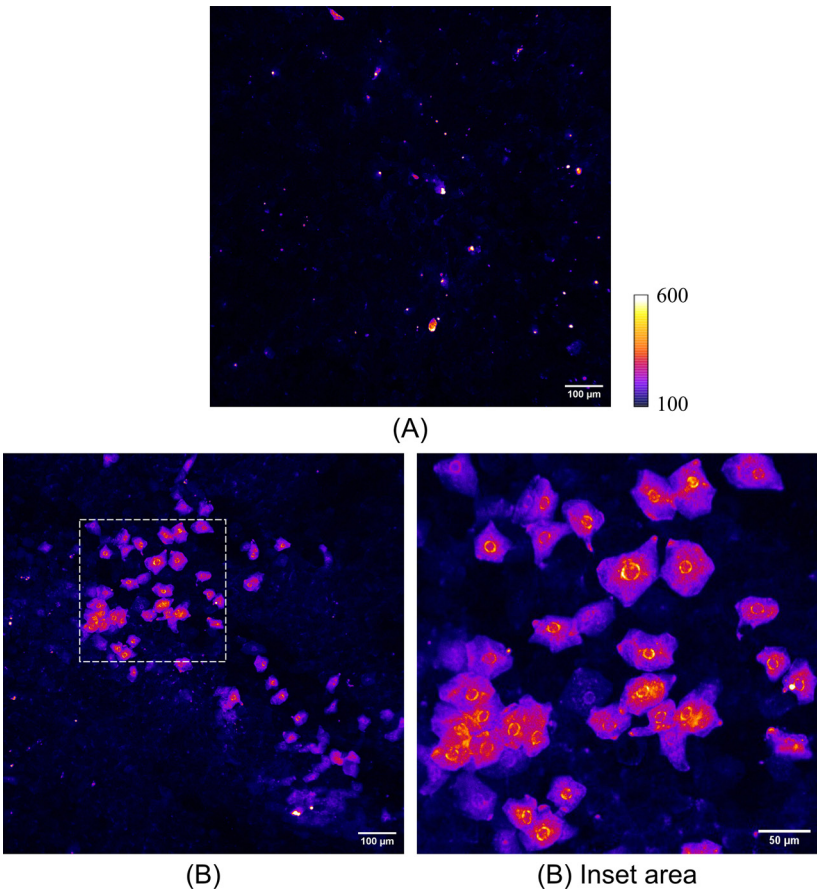

Fig. 9 Confocal microscope images of mucosal tissue treated with (A) an aqueous solution of RE-E1P47-Rho and (B) HG with RE-E1P47-Rho (systems A and B from Table 1). An inset in (B) provides a magnified view of a selected area. Images were processed with the ImageJ Fire filter. Both images represent the confocal plane with maximum intensity, with adjusted intensity values between 100 and 600 (on a scale of 0 to 65 535).

peptide within specific areas of the mucosal tissue. Fig. 10A presents a box plot of the logarithmic intensity values obtained from each confocal micrograph, using only the *Z*-plane with the highest intensity from each image stack. This visualization enables a comparison of the relative quantification of peptide permeation when applied with the HG *versus* the aqueous solution. Fig. 10B shows the *Z*-depth distances at which fluorescence, corresponding to peptide permeation, was detected in

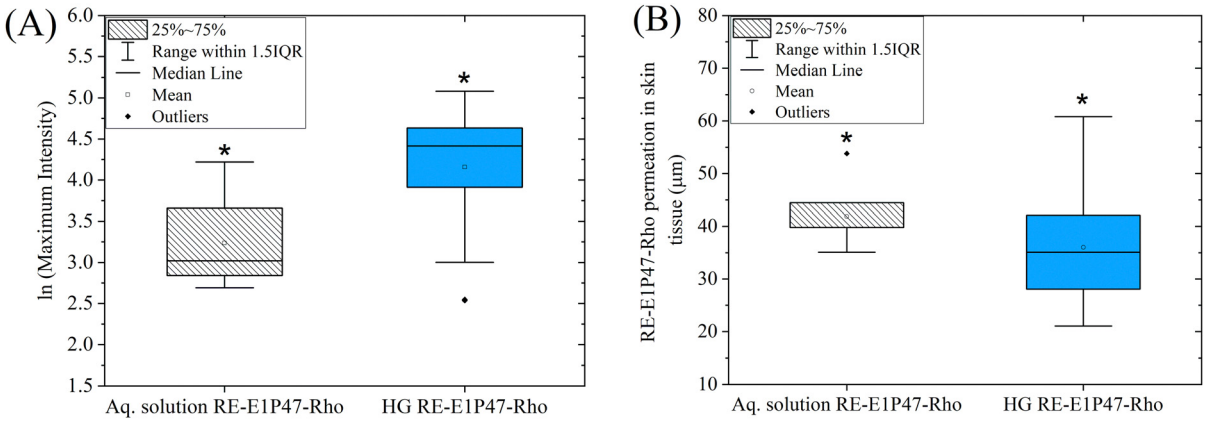

Fig. 10 (A) Box plot showing RE-E1P47-Rho permeation using the aqueous solution and the HG (systems A and B in Table 1), considering only the *Z*-plane with the highest intensity from each image stack. Significant differences were observed for both samples. (B) Graph representing the permeation depths (in μm) of RE-E1P47-Rho, also using only the *Z*-plane with the highest intensity from each stack. Confocal *Z*-plane images were acquired at 2.34 μm intervals along the *Z*-axis.

the various micrographs, again considering only the *Z*-plane with the highest intensity from each stack. The raw data for Fig. 10A and B are available in the ESI,† Tables S5 and S6, respectively.

In Fig. 9, when the peptide is applied with the aqueous solution, cells are not visible in the micrographs. Some spots are observed that may correspond to a small quantity of peptide aggregates that have absorbed in the mucosa surface but were not retained within the cells. In contrast, in Fig. 9B, the results from applying the peptide with the HG show well-defined cells and higher fluorescence intensity, indicating that the peptide is successfully taken up by the cells, localizing primarily in the nuclei and organelles.

The box plot results in Fig. 10A and B correlate with those in Fig. 8A and B. Regarding peptide permeation, Fig. 10A shows significant differences between the aqueous solution and HG application. The results demonstrate that the relative amount of peptide (considering only the *Z*-plane with the highest intensity in each micrograph) was greater when applied with the HG than with the aqueous solution (consistent with the results in Section 3.2.1). Concerning the peptide permeation depth, Fig. 10B illustrates how deeply the peptide penetrated the mucosa with the HG compared to the aqueous solution. The findings reveal that the peptide permeated deeper with the aqueous solution (~42 μm) than the HG (~36 μm), although the quantity retained in the mucosa for the aqueous solution was lower, as indicated in Fig. 10A. However, it is important to note that the confocal microscopy results of peptide permeation depth showed in Fig. 10B (~42 and 36 μm for aq. solution and HG respectively) are not directly comparable to those in Fig. 8B (~105 and 76 μm for aq. solution and HG respectively). Confocal microscopy has limitations for observing full-depth permeation in intact mucosal tissue, as the laser cannot penetrate deeply enough through the entire sample; it only excites the more superficial cells due to energy absorption within the tissue. This limitation explains the different depth values observed in Fig. 8B and 10B. Statistical analysis can be found in the ESI,† Tables S7 and S8.

In this section, in addition to quantifying intensity levels and permeation depths, we can observe where the peptide is retained within the non-keratinized squamous epithelial cells that make up the most superficial layer of the vaginal mucosa. The images reveal that the nuclei membranes are the most fluorescent areas, suggesting a significant accumulation of RE-E1P47-Rho there.

The lipid vesicles that form the HG structure interact with the lipid bilayer of epithelial cells, facilitating the peptide's entry into the cells. As shown in the inset of Fig. 9B, the nuclei exhibit high fluorescence intensity, which is attributed solely to the peptide, as no autofluorescence was detected in the tissue. As noted in Section 3.1 and in line with findings previously reported,[25] the peptide RE-E1P47 has the affinity to assemble into cell lipid bilayers. Our results suggest that the peptide not only permeates the cell membrane but also, once inside, may become associated with various organelles bound by lipid bilayers, including the nuclear membrane,[48] which also comprises a lipid bilayer.

In contrast, when the peptide is applied in an aqueous solution, it does not become retained within the cells (Fig. 9A). Instead, peptide aggregates are distributed along the surface of the mucosa. These aggregates represent the dispersed, lipophilic peptide in water, but they do not penetrate the cells, likely due to the absence of a lipid-based delivery system.

3.3. *Ex vivo* vaginal mucosa tissue efficacy assay with HIV-1 infection

As a proof of concept, we aim to determine the capacity of the HG to deliver the antiviral peptide and protect against HIV-1 infection in a well-established explant tissue model of cervicovaginal tissue.[34] For these experiments, the model was polarized[32,33] to resemble HIV-1 transmission at the female genital tract and samples were pre-incubated with HG RE-E1P47 and controls before HIV-1 *ex vivo* infection.

Results in Fig. 11A show the $CD8^-p24^+$T cell count per million $CD8^-$T cells from 4 different tested samples: the positive HIV control, the application of a HG control, the aqueous solution with RE-E1P47 and the HG with RE-E1P47. Fig. 11B shows the frequency of $CD8^-p24^+$ population normalized to the HIV+ infection condition (regarded as 100%) for each sample. Finally, Fig. 11C compares these normalized values (from Fig. 11B) between the aqueous solution and the HG loaded with RE-E1P47.

As shown in Fig. 11A, *ex vivo* infection with a high dose of HIV-1_{BAL} induced consistently high levels of HIV^-1^+ cells in all mucosal samples, as indicated by the expression of the viral protein p24 within the $CD8^-$T cell fraction measured by flow cytometry. Of note, the $CD8^-$T cell gate includes putative $CD4^+$T cells and also $CD4^+$ T cells that have downregulated CD4 expression, which is known to occur during productive HIV-1 infection.[49]

Compared to the HIV control, previous exposure to HG RE-E1P47 was the only treatment that effectively reduced the $CD8^-p24^+$ cell count per million $CD8^-$T cells (Fig. 11A), while the Aq. solution RE-E1P47 group, containing the peptide only, or the HG control, had no capacity to decrease productive infection. The median $CD8^-p24^+$ population in the Aq. solution RE-E1P47 group was similar to that in the HIV control, indicating minimal reduction in infection levels (185 679 against 153 414 $CD8^-p24^+$ cells per million $CD8^-$T cells, respectively). Of note, live $CD45^+$ cells across all samples and conditions ranged from 75% to 80% ensuring that the effectiveness of the anti-HIV pre-treatment is due to the peptide's action rather than cellular death. In Fig. 11B, treatment with Aq. Solution RE-E1P47 gave a moderate reduction of 19.67% due to the minimal reduction in infection levels. In contrast, treatment with HG RE-E1P47 resulted in a significant 61.47% reduction (p = 0.0098, Fig. 11B), with medians decreasing from 185 679 in the HIV control group to 74 035 in the HG RE-E1P47 group (p = 0.0078, Fig. 11A). Moreover, while sample size limited statistical significance, in Fig. 11C, a direct comparison is shown between the two treatment groups, revealing consistent reduction in the infection levels associated with HG RE-E1P47 pre-treatment. These results highlight the significant effectiveness of HG RE-

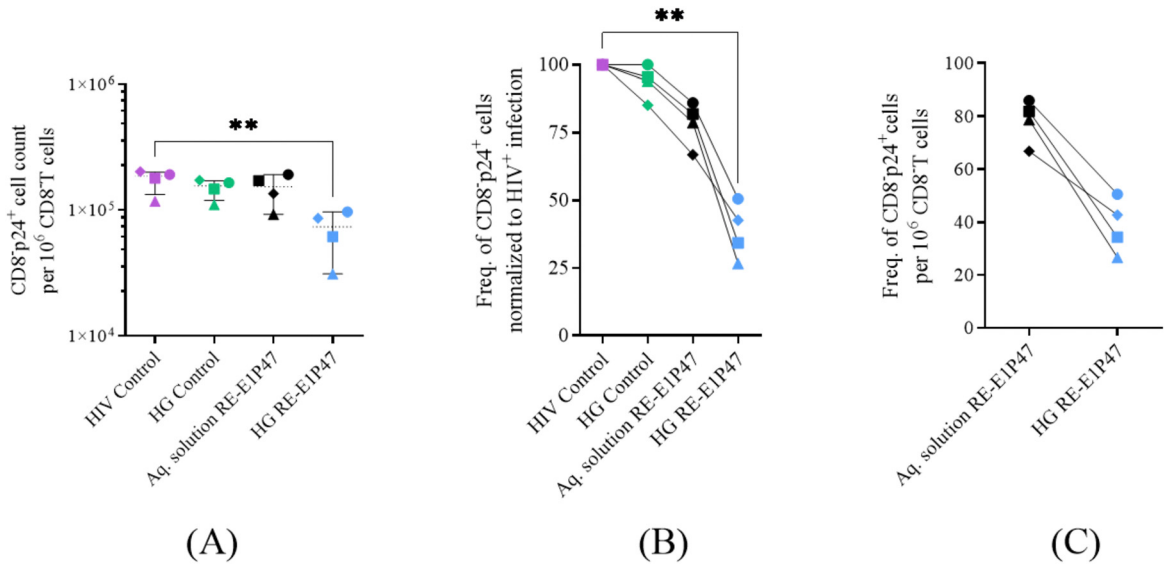

Fig. 11 (A) $CD8^{-}p24^{+}$T cell count per million $CD8^{-}$T cells comparing effects of aqueous solution (Aq. solution) and hydrogel (HG) formulations control/RE-E1P47. (B) Frequency of $CD8^{-}p24^{+}$ population normalized to the HIV^{+} infection condition for each sample (as the 100%). (C) Comparison among the frequency of $CD8^{-}p24^{+}$ population per million $CD8^{-}$T cells between the Aq. solution RE-E1P47 and HG RE-E1P47. Data are represented with the median with the interquartile range (A); each sample is represented by a unique shape, and each group is represented by a single color. Statistical comparisons using a non-parametric Friedman ANOVA test with Dunn's correction for multiple comparisons are shown: $**p < 0.01$.

E1P47 in limiting HIV-1 infection in the human cervicovaginal mucosa.

These significant efficacy results could be correlated with the confocal fluorescence microscopy results of full-mucosa tissue. RE-E1P47 is a fusion inhibitor peptide that specifically interferes with the N-terminal region of gp41 in HIV-1, and when RE-E1P47 assembles within a lipid bilayer membrane, it retains the active conformation required for interaction with its viral target site.[25] Fusion inhibitor peptides that interfere with critical domains of the gp41 protein in HIV-1 have to be embedded in membranes to properly interact with their viral target. The affinity of the peptide and subsequent assembly in the membrane is closely related to its antiviral activity.[50] However, in Section 3.2.2, it has been observed that RE-E1P47 is capable of entering cells and even localizing to the nuclear membrane when it is applied only with the HG, not the cell membrane. Rojekar *et al.*[51] and Chan *et al.*[52] describe the crucial role of the N-terminal region of gp41 in the process of HIV entry into host cells. The role of gp41 is mainly to facilitate the fusion of viral and cellular membranes for the entry of the viral content into the cell. After membrane fusion is complete, the gp41 protein remains in the host cell membrane as part of the viral proteins embedded in it. While in Section 3.2.2 it has been observed that RE-E1P47 is capable of entering cells and even localizing to the nuclear membrane (not the cell membrane, see yellow color in Fig. 9B), this does not appear to compromise its efficacy. We hypothesize that if the peptide is found within the cell, it is also likely present in the cell membrane. The nuclear envelope connects to the endoplasmic reticulum junctions that allow lipid exchange.[48] Lipids can laterally diffuse through membrane continuities that exist between the endoplasmatic reticulum and the outer and inner nuclear membrane.[53] Therefore, there may be some dynamic movement of RE-E1P47 between the lipid bilayer of the nucleus envelope, the endoplasmatic reticulum and the cell membrane.

Finally, the HG system in this study delivers RE-E1P47 to the mucosa surface layers, where it may interact with the epithelial cells, as has been observed in Fig. 9, making it a possible candidate for PrEP against HIV-1. Considering a real *in vivo* application, between 6.55 mL and 14.1 mL of HG would be needed to cover the surface of a vagina, depending on its size.[54] To validate this, future dosing studies would be required. When applying HG *in vivo* in excess, part of the lipids would integrate with the natural components of the mucosa, while the extra HG would drain externally as part of the vaginal fluid. Further analysis is needed to clearly define the final location of the HG lipids. Additional future studies should consider that transmucosal permeation involves variables, such as physico-dynamic conditions, osmolarity, pH effects (both environmental and HG), muco-adhesiveness, any irritation, *etc.* The study of these variables will help to understand aspects to optimize the use of this material.

4. Conclusions

In this work, a lipid-based HG incorporating the RE-E1P47 peptide has been proposed for female genital tract application as a candidate for PrEP against HIV-1. The target peptide inhibits the membrane fusion step of HIV entry into host cells, thereby preventing (or limiting) the infection of target cells. Characterization studies show the peptide's localization within the HG structure, highlighting its affinity for lipid bilayers due to its lipophilic nature and no interaction or diffusion with the

VFS. In addition, the incorporation of the peptide does not change the organization of lipids in the HG formula. When the peptide is applied topically to the mucosal surface, its aqueous solution is ineffective and does not permeate adequately. However, when delivered *via* the HG, the peptide is retained in the outer layers of the epithelium, particularly within the epithelial cells. Consequently, a significant reduction in HIV-1 infection has been demonstrated when the HG is applied several hours before infection. In conclusion, this lipid-based HG loaded with RE-EP147 is a promising candidate for further in-depth studies as PrEP strategies against HIV-1. Additionally, the HG has potential for treating various fungal or bacterial infections when formulated with the appropriate active molecules for biomedical applications.

Data availability

The data supporting this article, including Fig. 8 and 10 (with the statistical results), has been included as part of the ESI.† Other data files are available upon request to the corresponding author due to confidentiality requirements.

Conflicts of interest

Author Noèlia Loza-Rodríguez was employed by the company Bicosome S. L. The remaining authors declare that the research was conducted in the absence of any commercial or financial relationships that could be construed as a potential conflict of interest. Data collected from human participants are not available for confidentiality reasons.

Acknowledgements

The authors are grateful to Dr Tania García Becerra from the Molecular Imaging Platform in the IBMB-CSIC for her expert technical assistance. We are also thankful for the University of Barcelona's Scientific and Technological Centers (CCiTUB), specifically Dr Manel Bosch from Advanced Optic Microscopy for the technical assistance, Cryostat service, and for kindly supply the Hoechst and WGA488 fluorescent dyes. We also thank Jaume Caelles from the SAXS-WAXS service and Nicole Conde for ATR-FTIR technical assistance. To Lipoid GmbH and Abaran Materias Primas, provided HSPC and DOTAP and the Veterinary Faculty of Autonomous University of Barcelona, specifically Jose Luis Ruiz de la Torre and Lola Perez, for kindly providing the ovine mucosal tissues. We would like to thank all the patients who participated in the efficacy study and their providers, including Drs. Laura Mañalich-Barrachina and Josep Castellví for sample collection. This work was supported by funds from the Spanish Ministry of Science and Innovation with Ayudas para contratos para la formación de doctores en empresas ''Doctorados Industriales'', DIN2019-010777, Bicosome S. L., the Mechanism for the Recovery and Resilience of the European Union and MICINN with the CPP2021-008954 project and PID2021-124848OB-I00 project. This work was also supported by grants from the Spanish Health Institute Carlos III (ISCIII, PI20/00160), cofunded by ERDF/ESF, ''A way to make Europe''/''Investing in your future'', from MCIN/AEI/10.13039/501100011033 and the European Union ''Next Generation EU''/PRTR (CNS2022-135549 and PID2023-149204OB-I00), the Fundació La Marató TV3 (201814-10 FMTV3) and Gilead fellowships (GLD21/00049 and GLD23/00012) to M. G. M. J. G. and I. H. acknowledge the Grant PID2021-122216-OB-I00 received from the Spanish Ministry of Science, Innovation and Universities and the European Regional Development Fund.

References

1 A. M. Dos Santos, S. G. Carvalho, V. H. S. Araujo, G. C. Carvalho, M. P. D. Gremião and M. Chorilli, *Int. J. Pharm.*, 2020, **590**, 119867.
2 L. C. Rohan and A. B. Sassi, *AAPS J.*, 2009, **11**, 78.
3 T. Osmałek, A. Froelich, B. Jadach, A. Tatarek, P. Gadziński, A. Falana, K. Gralińska, M. Ekert, V. Puri, J. Wrotyńska-Barczyńska and B. Michniak-Kohn, *Pharmaceutics*, 2021, **13**, 884.
4 A. D. Van Eyk, P. Van Der Bijl and L. M. Moll, *Eur. J. Inflamm.*, 2008, **6**, 65–71.
5 C. Prego, M. García, D. Torres and M. J. Alonso, *J. Controlled Release*, 2005, **101**, 151–162.
6 C. A. Squier, M. J. Mantz, P. M. Schlievert and C. C. Davis, *J. Pharm. Sci.*, 2008, **97**, 9–21.
7 B. Valamla, P. Thakor, R. Phuse, M. Dalvi, P. Kharat, A. Kumar, D. Panwar, S. B. Singh, P. Giorgia and N. K. Mehra, *J. Drug Delivery Sci. Technol.*, 2022, **70**, 103162.
8 M. M. El-Hammadi and J. L. Arias, in *Theory and Applications of Nonparenteral Nanomedicines*, ed. P. Kesharwani, S. Taurin and K. Greish, Academic Press, 2021, pp. 235–257.
9 R. Sanz, A. C. Calpena, M. Mallandrich and B. Clares, *Curr. Pharm. Des.*, 2015, **21**, 2867–2882.
10 M. Ariza-Sáenz, M. Espina, A. Calpena, M. J. Gómara, I. Pérez-Pomeda, I. Haro and M. L. García, *Mol. Pharm.*, 2018, **15**, 5005–5018.
11 R. Sanz, B. Clares, M. Mallandrich, J. Suñer-Carbó, M. J. Montes and A. C. Calpena, *Int. J. Pharm.*, 2018, **535**, 393–401.
12 Q. Abdool Karim, S. S. Abdool Karim, J. A. Frohlich, A. C. Grobler, C. Baxter, L. E. Mansoor, A. B. M. Kharsany, S. Sibeko, K. P. Mlisana, Z. Omar, T. N. Gengiah, S. Maarschalk, N. Arulappan, M. Mlotshwa, L. Morris and D. Taylor, *Science*, 2010, **329**, 1168–1174.
13 M. Jose Gomara and I. Haro, *Curr. Med. Chem.*, 2014, **21**, 1188–1200.
14 M. J. Gómara, V. Sánchez-Merino, A. Paús, A. Merino-Mansilla, J. M. Gatell, E. Yuste and I. Haro, *Biochim. Biophys. Acta, Gen. Subj.*, 2016, **1860**, 1139–1148.
15 Y. Pérez, M. J. Gómara, E. Yuste, P. Gómez-Gutierrez, J. J. Pérez and I. Haro, *Chem. – Eur. J.*, 2017, **23**, 11703–11713.
16 M. J. Gómara, I. Pérez-Pomeda, J. M. Gatell, V. Sánchez-Merino, E. Yuste and I. Haro, *Nanomedicine*, 2017, **13**, 601–609.

17 M. Ariza-Sáenz, M. Espina, N. Bolaños, A. C. Calpena, M. J. Gomara, I. Haro and M. L. García, *Eur. J. Pharm. Biopharm.*, 2017, **120**, 98–106.
18 M. J. Gómara, R. Pons, C. Herrera, P. Ziprin and I. Haro, *Bioconjugate Chem.*, 2021, **32**, 1999–2013.
19 E. Sánchez-López, A. Paús, I. Pérez-Pomeda, A. Calpena, I. Haro and M. J. Gómara, *Pharmaceutics*, 2020, **12**, 502.
20 N. Loza-Rodríguez, A. Millán-Sánchez and O. López, *Eur. J. Pharm. Biopharm.*, 2023, **190**, 24–34.
21 K. Talló, O. López and V. Moner, WO2020/079302A2, 2020.
22 K. Talló, R. Pons, O. López, M. Bosch, M. Bosch and M. Cocera, *J. Mater. Chem. B*, 2020, **8**, 161–167.
23 K. Talló, S. Vílchez, R. Pons and O. López, *J. Mol. Liq.*, 2021, **322**, 114957.
24 N. Loza-Rodríguez, A. Millán-Sánchez, M. Mallandrich, A. C. Calpena and O. López, *Pharmaceutics*, 2024, **16**, 1187.
25 M. J. Gomara, Y. Perez, P. Gomez-Gutierrez, C. Herrera, P. Ziprin, J. P. Martinez, A. Meyerhans, J. J. Perez and I. Haro, *Sci. Rep.*, 2020, **10**, 14430.
26 P. Colombo, S. Cagnani, F. Sonvico, P. Santi, P. Russo and G. Colombo, in *Comprehensive Medicinal Chemistry II*, ed. J. B. Taylor and D. J. Triggle, Elsevier, Oxford, 2013, pp. 279–299.
27 T. Tsiligianni, A. Karagiannidis, P. Brikas and P. Saratsis, *Theriogenology*, 2001, **55**, 629–640.
28 K. Talló, R. Pons, C. González and O. López, *J. Mater. Chem. B*, 2021, **9**, 7472–7481.
29 N. Loza-Rodríguez, A. Millán-Sánchez and O. López, *Gels*, 2023, **9**, 649.
30 W. L. Bragg, *Proc. Cambridge Philos. Soc.*, 1929, **17**, 43–57.
31 J. Cantero and M. Genescà, *J. Immunol. Methods*, 2018, **460**, 26–35.
32 S. R. Abner, P. C. Guenthner, J. Guarner, K. A. Hancock, J. E. Cummins Jr., A. Fink, G. T. Gilmore, C. Staley, A. Ward, O. Ali, S. Binderow, S. Cohen, L. A. Grohskopf, L. Paxton, C. E. Hart and C. S. Dezzutti, *J. Infect. Dis.*, 2005, **192**, 1545–1556.
33 L. A. Ouattara, N. C. Vann and G. F. Doncel, in *HIV Reservoirs: Methods and Protocols*, ed. G. Poli, E. Vicenzi and F. Romerio, Springer US, New York, NY, 2022, pp. 157–172.
34 J. Cantero-Pérez, J. Grau-Expósito, C. Serra-Peinado, D. A. Rosero, L. Luque-Ballesteros, A. Astorga-Gamaza, J. Castellví, T. Sanhueza, G. Tapia, B. Lloveras, M. A. Fernández, J. G. Prado, J. M. Solé-Sedeno, A. Tarrats, C. Lecumberri, L. Mañalich-Barrachina, C. Centeno-Mediavilla, V. Falcó, M. J. Buzon and M. Genescà, *Nat. Commun.*, 2019, **10**, 4739.
35 G. Rodríguez, M. C. Cócera, L. Rubio, C. López-Iglesias, R. Pons, A. De La Maza and O. López, *Mol. Pharm.*, 2012, **9**, 482–491.
36 B. C. Smith, *Spectroscopy*, 2016, **31**, 14–21.
37 B. L. Mojet, S. D. Ebbesen and L. Lefferts, *Chem. Soc. Rev.*, 2010, **39**, 4643–4655.
38 A. Alinaghi, M. R. Rouini, F. Johari Daha and H. R. Moghimi, *Int. J. Pharm.*, 2014, **459**, 30–39.
39 R. B. Campbell, S. V. Balasubramanian and R. M. Straubinger, *Biochim. Biophys. Acta, Biomembr.*, 2001, **1512**, 27–39.
40 D. M. Small, *J. Lipid Res.*, 1984, **25**, 1490–1500.
41 H. M. Alhelal, S. Mehta, V. Kadian, V. Kakkar, H. Tanwar, R. Rao, B. Aldhubiab, N. Sreeharsha, P. Shinu and A. B. Nair, *Gels*, 2023, **9**, 576.
42 K. L. Vincent, N. Bourne, B. A. Bell, G. Vargas, A. Tan, D. Cowan, L. R. Stanberry, S. L. Rosenthal and M. Motamedi, *Sexually Trans. Diseases*, 2009, **36**, 312.
43 K. L. Vincent, G. Vargas, J. Wei, N. Bourne and M. Motamedi, *Am. J. Obstet. Gynecol.*, 2013, **208**, 282.e1.
44 S. Mehta, H. Verstraelen, K. Peremans, G. Villeirs, S. Vermeire, F. De Vos, E. Mehuys, J. P. Remon and C. Vervaet, *Int. J. Pharm.*, 2012, **426**, 44–53.
45 J. A. Moss, A. M. Malone, T. J. Smith, S. Kennedy, E. Kopin, C. Nguyen, J. Gilman, I. Butkyavichene, K. L. Vincent, M. Motamedi, D. R. Friend, M. R. Clark and M. M. Baum, *Antimicrob. Agents Chemother.*, 2012, **56**, 875–882.
46 C. Alonso, M. Martí, A. Ramos, A. C. Calpena, B. Clares-Naveros and L. Coderch, *Membranes*, 2023, **13**, 905.
47 Y.-Q. Yu, X. Yang, X.-F. Wu and Y.-B. Fan, *Front. Bioeng. Biotechnol.*, 2021, **9**, 646554.
48 A. Romanauska and A. Köhler, *Nat. Cell Biol.*, 2023, **25**, 1290–1302.
49 N. Michel, I. Allespach, S. Venzke, O. T. Fackler and O. T. Keppler, *Curr. Biol.*, 2005, **15**, 714–723.
50 M. J. Gomara, Y. Perez, J. P. Martinez, R. Barnadas-Rodriguez, A. Schultz, H. von Briesen, A. Peralvarez-Marin, A. Meyerhans and I. Haro, *Sci. Rep.*, 2019, **9**, 3257.
51 S. Rojekar, A. D. Gholap, N. Togre, P. Bhoj, C. Haeck, N. Hatvate, N. Singh, J. Vitore, S. Dhoble, S. Kashid and V. Patravale, *J. Controlled Release*, 2024, **372**, 494–521.
52 D. C. Chan and P. S. Kim, *Cell*, 1998, **93**, 681–684.
53 G. van Meer, D. R. Voelker and G. W. Feigenson, *Nat. Rev. Mol. Cell Biol.*, 2008, **9**, 112–124.
54 J. López-Olmos, *Clin. Invest. Ginecol. Obstet*, 2005, **32**, 230–243.